Available online at www.sciencedirect.com
SCIENCE DIRECT®
Journal of Magnetic Resonance 168 (2004) 46–52
JMR Journal of Magnetic Resonance
www.elsevier.com/locate/jmr

Reduced apparent longitudinal relaxation times in slice-selective experiments in strong magnetic field gradients

Nikolaus Nestle,[a,*] Bernadeta Walaszek,[b] and Markus Nolte[a]

[a] *Institut für Festkörperphysik, TU Darmstadt, Hochschulstraße 6, D-64289 Darmstadt, Germany*
[b] *Marian Smoluchowksi Institute of Physics, Jagiellonian University of Kraków, 16, ul. Reymonta 4, PL-30-059 Kraków, Poland*

Received 20 December 2003; revised 23 January 2004

Abstract

In contrast to transverse nuclear magnetizations, longitudinal spin magnetizations are usually considered as insensitive to magnetic field gradients. While this assumption is valid for homogeneously excited samples, the apparent longitudinal spin relaxation behavior of thin magnetization slices in high magnetic fields is strongly modified by diffusion. In this contribution, we present the results of theoretical and experimental studies on this effect. Furthermore, possible applications and the impact on different types of NMR techniques using strong magnetic field gradients are discussed.

Keywords: Longitudinal relaxation; Strong gradient; Diffusion; Slice-selective excitation

1. Introduction

The sensitivity of transverse nuclear spin magnetizations to magnetic field gradients has been known since the early days of NMR. A quantitative description of the interaction of a transverse nuclear spin magnetization with a magnetic field gradient was already given by Hahn in his report on the spin echo [1]. On the basis of this effect, various protocols for measuring diffusion coefficients have been developed [2–6] which are among the most precise and detailed techniques for measuring self-diffusion coefficients available today.

Longitudinal magnetizations, by contrast, are usually considered to be insensitive to the action of magnetic field gradients. The insensitivity of longitudinal magnetizations to magnetic field gradients is for example used in the application of spoiler gradients [7] in multiquantum NMR spectroscopy and many MRI techniques.

The combined effect of magnetic field gradients and molecular motion on longitudinal magnetizations is used in inflow–utflow and tagging techniques for flow-encoding in MRI [8,9] and also several approaches to measuring diffusion by observing the diffusive decay of a magnetization grid [10,11] were suggested. In non-imaging experiments, the impact of diffusive motion in magnetic field gradients on the longitudinal magnetization is usually neglected. While this is appropriate in homogeneously excited samples, considerable diffusion effects can be observed in the presence of static magnetic field gradients in which the excitation of the sample is typically restricted to a thin resonant slice [12].

2. Magnetization recovery in thin excited sample slices

Irradiation of an RF pulse in the presence of a magnetic field gradient leads to a selective excitation of nuclear spins in the region of resonant Larmor frequencies. The strength of the excitation at a point with a given Larmor frequency corresponds to the amplitude of the respective frequency in the RF pulse. The distribution of amplitude over frequency $I(f)$ (and thus a corresponding spatial excitation profile $P(x)$) for an RF pulse with maximal amplitude A_0 and centre frequency f_0 is determined by the Fourier transform of the envelope $A(t)$ of the pulse in the time domain.

* Corresponding author. Fax: +49-6151-16-2883.
E-mail address: nikolaus.nestle@physik.tu-darmstadt.de (N. Nestle).

1090-7807/$ - see front matter © 2004 Elsevier Inc. All rights reserved.
doi:10.1016/j.jmr.2004.01.014

$$I(f) = \frac{1}{\sqrt{2\pi}} \int_{-\infty}^{\infty} A(t) \exp(\mathrm{i}ft)\, \mathrm{d}t. \quad (1)$$

A rectangular pulse envelope therefore leads to a sinc-shaped excitation profile in space, by contrast, a sinc-shaped pulse envelope in time leads to a rectangular profile in space. A Gaussian pulse shape in time leads to a Gaussian excitation profile in space. The relationship between pulse shapes and the resulting excitation profiles in space has been extensively studied in the context of MRI [9,13].

First we consider a non-imaging experiment on a spatially homogeneous sample with a uniform equilibrium magnetization, M_0. In the absence of motion, the excited slice profile, $P(x)$, has no influence in measuring any magnetization-recovery process that can be described by an expression of the form

$$\begin{aligned} M(x,t) &= M_0 - \Delta M(x) F(t) \\ &= M_0 - M_0 P(x) F(t) \end{aligned} \quad (2)$$

(with $F(t)$ denoting an arbitrary function of time, e.g., an exponential decay).

The magnetization recovery is measured in an experiment of the type (excitation pulse) – (variable delay) – (sampling pulse) – (detection of signal $S(t)$). This signal $S(t)$ measured after the sampling pulse is given as the spatial average of $\langle \Delta M(x) F(t) P(x) \rangle_x$ over the excitation profile

$$\begin{aligned} S(t) &= \langle \Delta M(x) F(t) P(x) \rangle_x \\ &= M_0 \langle P(x) P(x) F(t) \rangle_x \\ &= M_0 \langle P(x) P(x) \rangle_x F(t) \\ &= M_0 Q F(t) \end{aligned} \quad (3)$$

with $Q = \langle P(x) P(x) \rangle_x$ denoting a constant factor. This even holds true if the slice profiles of the exciting pulse and the sampling pulse are different.

This separation of the spatial and temporal effect is not possible any more in the presence of motion. The most important type of motion that has to be considered in this case is (free) diffusion. Diffusion of the excited molecules leads to a broadening and blurring of the initially excited slice profile which is given as the solution of the diffusion equation

$$\frac{\partial C(x,t)}{\partial t} = D \frac{\partial^2 C(x,t)}{\partial x^2} \quad (4)$$

with $C(x,t) = \Delta M(x,t)/M_0$ the initial condition $C(x,0) = P(x)$.

General methods for solving the diffusion equation for arbitrary initial conditions are discussed, e.g., in the book by Crank [14]. For most cases, the resulting expressions are analytically quite complicated. A simple case is the temporal development of a Gaussian excitation profile with the width $2b$ (variance b^2). It can be computed from the well-known solution for a δ-shaped initial concentration profile by introducing a time-shift t_b:

$$C(x,t) = \frac{C_0}{2\sqrt{\pi(D(t+t_b))}} \exp\left(-\frac{x^2}{4D(t+t_b)} \right) \quad (5)$$

comparing $4Dt_b$ and $2b^2$ at zero time, we find $t_b = b^2/2D$ or

$$C(x,t) = \frac{C_0}{2\sqrt{\pi(Dt + b^2/2)}} \exp\left(-\frac{x^2}{4Dt + 2b^2} \right). \quad (6)$$

Another relatively simple solution is that for an initially rectangular excitation profile with the width $2b$:

$$C(x,t) = \frac{1}{2} C_0 \left(\mathrm{erf}\left(\frac{b-x}{2\sqrt{Dt}} \right) + \mathrm{erf}\left(\frac{b+x}{2\sqrt{Dt}} \right) \right). \quad (7)$$

The development for both excitation profiles with time is plotted in Fig. 1. Sampling of a diffusively broadening excitation profile $C(x,t)$ by an excitation pulse with the profile $P(x)$ at different times cannot be described by a constant factor Q any more. Instead, the spatial averaging of the signal has to be done anew for each delay time and can be described by a balance factor.

$$B(t) = \frac{\langle C(x,t) P(x) \rangle_x}{\langle P(x) P(x) \rangle_x}. \quad (8)$$

$C(x,t)P(x)$ is plotted for the longest diffusion time along with the curves $C(x,t)$ in the graphs in Fig. 1 ($P(x)$ is assumed to be identical to $C(x,0)$ in the following

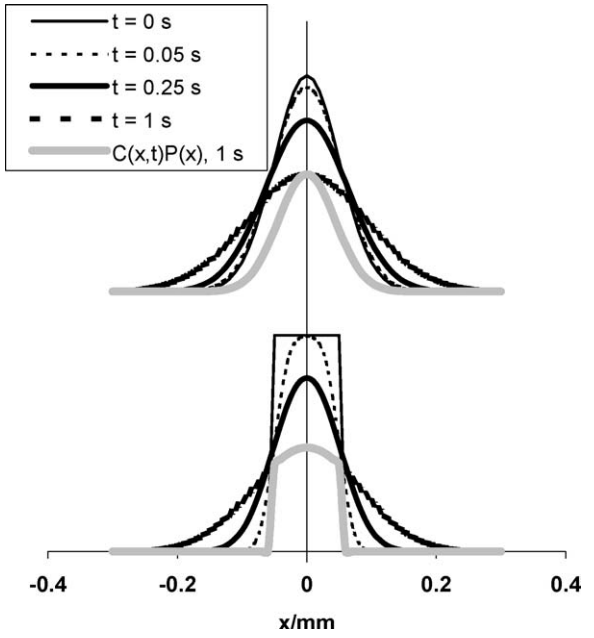

Fig. 1. Diffusive spreading $C(x,t)$ of excited magnetization after selective excitation $P(x)$ with a Gaussian (above) or a rectangular slice profile. For the longest diffusion time, the magnetization still residing available within the original slice profile is given, too ($D = 3 \times 10^{-9}\,\mathrm{m^2\,s^{-1}}$).

discussion. This is the case for identical RF pulses for excitation and sampling). Using the balance factor $B(t)$, the magnetization-recovery curve takes the form

$$\langle M(t)\rangle_x = M_0(1 - QB(t)F(t)). \tag{9}$$

In Fig. 2, the factor $B(t)$ is plotted both for the Gaussian and the rectangular slice profile and for two different slice thicknesses. For the Gaussian excitation profile (see Eq. (6)), $B(t)$ can be computed analytically:

$$B(t) = \frac{\int_{-\infty}^{\infty} \frac{C_0}{2\sqrt{\pi D(t+t_b)}} e^{-\frac{x^2}{4D(t+t_b)}} \frac{C_0}{2\sqrt{\pi D t_b}} e^{-\frac{x^2}{4Dt_b}} dx}{\int_{-\infty}^{\infty} \left(\frac{C_0}{2\sqrt{\pi D t_b}} e^{-\frac{x^2}{4Dt_b}}\right)^2 dx}$$
$$= \frac{1}{\sqrt{1 + t/2t_b}} = \frac{1}{\sqrt{1 + Dt/b^2}}. \tag{10}$$

Computation of $B(t)$ for a rectangular excited slice profile (see Eq. (7)) is also possible; however, the resulting expression cannot be simplified to elementary functions as it is the case for the Gaussian profile. The expression for $B(t)$ in the case of a rectangular profile is:

$$B(t) = \frac{2\sqrt{Dt}}{b\sqrt{\pi}}\left(e^{-b^2/4Dt} - 1\right) + \mathrm{erf}\left(\frac{b}{2\sqrt{Dt}}\right). \tag{11}$$

If $F(t)$ is a simple exponential relaxation curve, the magnetization-recovery curve with the diffusion-balance correction term for a Gaussian profile takes a simple analytical from:

$$\langle M(t)\rangle_x = M_0\left(1 - Q\frac{\exp(-t/T_1)}{\sqrt{1 + Dt/b^2}}\right). \tag{12}$$

The corresponding magnetization curve is plotted for several values of b in Fig. 3. In the same figure, also the analytically more complicated magnetization curves for a rectangular profile are given. Note the initially more

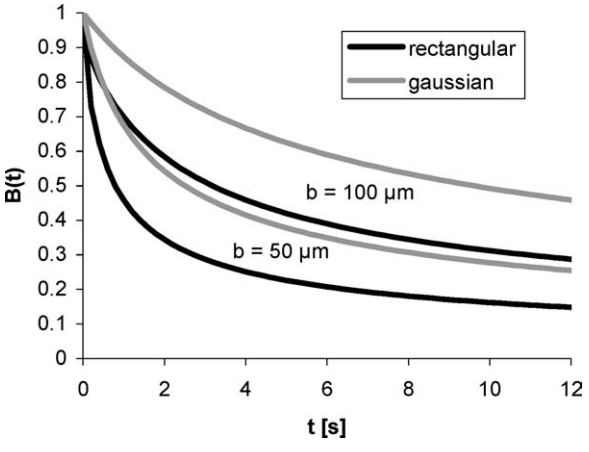

Fig. 2. Examples for $B(t)$ computed for a Gaussian and rectangular slice profiles and assuming $D = 3 \times 10^{-9}\,\mathrm{m^2\,s^{-1}}$. The lower two curves correspond to a nominal slice thickness of 50 µm, the upper two curves to 100 µm. Note the initially faster decrease of $B(t)$ for the rectangular profiles.

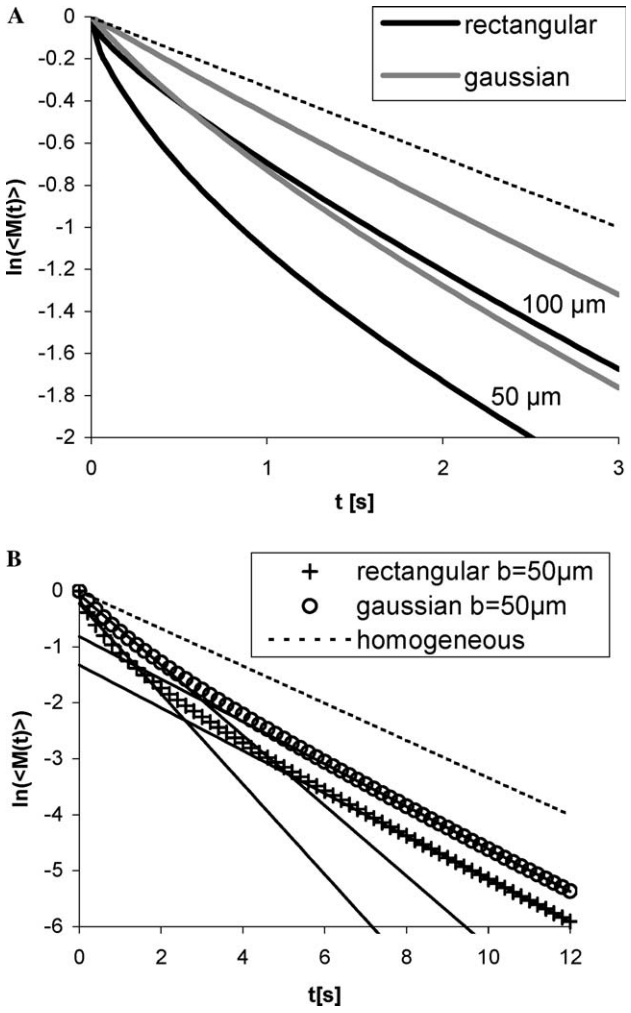

Fig. 3. Calculated influence of diffusion on the magnetization-recovery curves ($D = 3 \times 10^{-9}\,\mathrm{m^2\,s^{-1}}$, $T_1 = 3\,\mathrm{s}$). (A) Short-time behavior for two different slice thicknesses. (B) Long-time behavior: After a diffusion-dominated initial phase, the magnetization-recovery curves become more and more exponential and dominated by relaxation. The slope of the thin solid lines fitted by linear regression to the longtime tail only deviates by about 10% from the "real" longitudinal relaxation rate while the initial slope of the line fitted to the initial part of the 50 µm curve is more than twice as high.

pronounced decay of the magnetization for the rectangular slices compared to the Gaussian slices of the same nominal thickness. The fast initial decay of the magnetization in a rectangular slice profile cannot be approximated by an exponential decay as it is possible for the Gaussian slice profile. Comparing the signal decay at longer times, the slopes of the curves become more and more similar. The decreasing influence of the diffusion effect at long magnetization-recovery times can be expected as the mean diffusive shift only grows with the square root of time. Therefore, longitudinal relaxation with the bulk relaxation rate prevails for long magnetization-recovery times.

For $t \ll b^2/D$, this expression can be simplified even more by means of a Taylor expansion:

$$\begin{aligned}\ln(M_0 - \langle M(t)\rangle_x) &= \ln(QB(t)e^{-t/T_1}) \\ &= \ln Q + \ln\left(B(t) - \frac{t}{T_1}\right) \\ &\approx \ln Q + \left(\frac{1}{B(t)}\frac{dB(t)}{dt}\right)\Big|_{t=0} t - \frac{t}{T_1} \\ &= \ln Q - \frac{D}{2b^2}t - \frac{t}{T_1} = \ln Q - \frac{t}{T_{1\text{Diff}}}\end{aligned} \tag{13}$$

with $T_{1\text{Diff}}$ denoting an effective relaxation time given as

$$\frac{1}{T_{1\text{Diff}}} = \frac{1}{T_1} + \frac{D}{2b^2}. \tag{14}$$

It can be easily shown that even for $t = 0.5b^2/D$, the relative error of $B(t)$ and the Taylor expansion is only 10%. For simple liquids with diffusion coefficients on the order of $10^{-9}\,m^2\,s^{-1}$ and excited slice thicknesses on the order of magnitude of 100 μm, $0.5b^2/D$ is on the order of several 100 ms and so the experimentally observable magnetization-recovery curves exhibit a nearly exponential behavior (see Fig. 4 and Table 1). A similar Taylor expansion for the case of a rectangular slice profile is not possible as the expression for $B(t)$ (see Eq. (11)) in this case exhibits a diverging slope for $t = 0$.

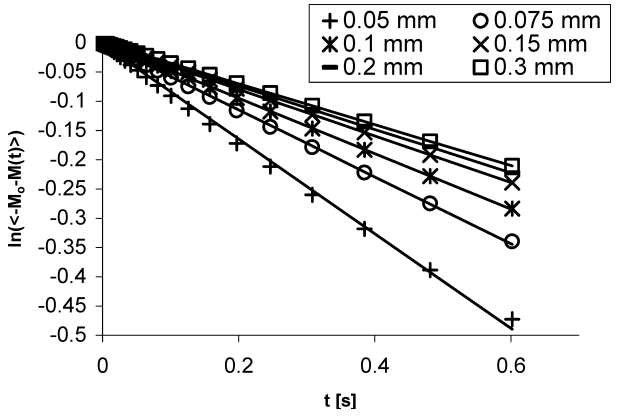

Fig. 4. Calculated magnetization-recovery curves for a Gaussian slice profile (assuming again $D = 3 \times 10^{-9}\,m^2\,s^{-1}$, $T_1 = 3$ s). The thin solid lines represent single exponential curves fitted by linear regression to the calculated curves. Except for the thinnest slice thickness, all magnetization-recovery curves exhibit only minor deviations from exponential behavior. The "relaxation times" determined from the slope of the respective curves (see Table 1) differ by more than a factor of 2.

Table 1
Relaxation times $T_{1\text{Diff}}$ determined in fits on the calculated data of Fig. 4

b (mm)	0.05	0.075	0.1	0.15	0.2	0.3
$T_{1\text{Diff}}$ (s)	1.24	1.75	2.11	2.51	2.7	2.86

3. Materials and methods

Slice-selective magnetization-recovery experiments were performed in a superconducting gradient magnet dedicated for static field gradient diffusometry [15]. The experiments were conducted at a proton resonance frequency of 99.55 MHz. In the magnet used in the experiments, the magnetic field corresponding to this resonance frequency is available at two different positions with static local magnetic field gradients of 161 and $59\,T\,m^{-1}$, respectively. (The gradient was calibrated in Hahn echo experiments on the water sample using the diffusion coefficient data provided in [16].)

The probehead used in the experiments was equipped with a horizontally oriented solenoidal coil with six windings in which the samples were inserted in 5 mm sealed glass tubes with a length of about 25 mm. The probehead was housed in an Oxford CFG-1200 evaporation cryostat system that allows experiments in a temperature range of 100–620 K when used with liquid nitrogen.

In order to ensure constant excitation profiles in all pulses, we used the very simple pulse sequence depicted in Fig. 5 for measuring T_1. The magnetization-recovery delay t between the first two α-pulses was varied in 40–60 steps from some milliseconds to several seconds. Using the same pulse width for excitation and for the readout of the recovered magnetization ensures identical profiles of both pulses which keeps interpretation of the data as simple as possible. The third α-pulse is used to generate an echo at $t + 2\tau$ by which $M(t)$ is measured. Measuring the FID directly after the second pulse was not possible due to the very short T_2^* resulting from the strong gradient and the receiver dead time. The echoes were acquired in quadrature detection and after correction of possible offsets, the absolute value of $M(t)$ was determined. For this data evaluation procedure, a python [17] script was used.

The samples used in our experiments were

- Ordinary dematerialized water (at 298 and 360 K),
- PDMS with a molecular weight of 17,000 Da.

The amplitude profile of the RF pulses used in the experiments was roughly rectangular in time. Such an RF pulse leads of course neither to a Gaussian nor to a rectangular excitation profile but to a sinc-shaped. However, comparing the central region of a sinc profile

Fig. 5. Echo-detected saturation-recovery sequence used for slice-selective relaxation time measurement in a static magnetic field gradient. The pulse angle α was determined from maximizing the signal intensity in a spin-echo experiment.

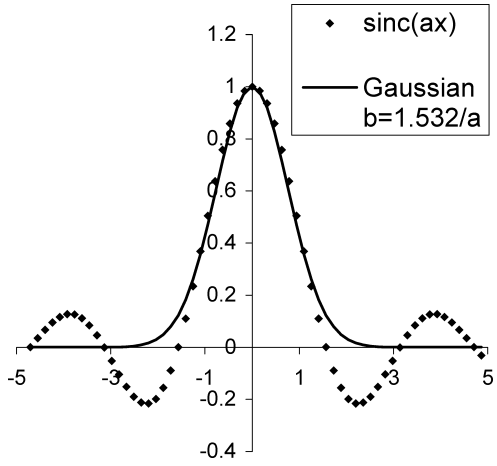

Fig. 6. Approximation of the central peak of a sinc function by a Gaussian.

with a Gaussian profile, it can be computed that the sinc-profile $P(x) = \frac{\sin(ax)}{ax}$ can be approximated quite well by a Gaussian profile with a slice thickness $b = c/a$ with $c = 1.532$ (see Fig. 6). The width of the Gaussian was determined by minimizing the integral of the square of the distance between the two curves over the interval $[-\pi/a, \pi/a]$ numerically in MAPLE.

4. Results and discussion

In Fig. 7, the experimentally recorded magnetization-recovery curves obtained with the pulse sequence sketched in Fig. 5 are given for various slice thicknesses (achieved by varying the duration of the α-pulse and correspondingly the power level of the RF transmitter). The observed magnetization-recovery behavior follows the expectations on the basis of the theoretical model for a Gaussian slice profile. Due to the very low signal intensity (and corresponding poor signal/noise ratio) associated with the smallest slice thickness, a fully quantitative evaluation of the curves on the basis of an unrestricted fit of Eq. (12) to the data is problematic. Similarly, the deviations from a monoexponential decay are only minor for the two shortest pulse lengths so that fitting these curves with a non-exponential model also proved numerically unstable.

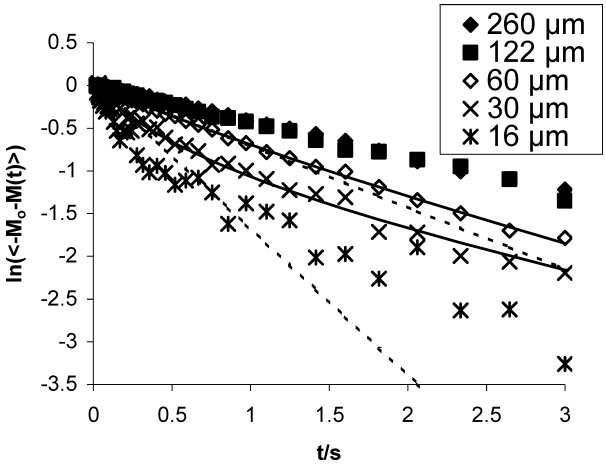

Fig. 7. Experimentally observed magnetization-recovery curves of a water sample ($T_1 = 2.9$ s) at 298 K and different pulse lengths. For the data obtained at pulse lengths 6.5 and 12.8 µs, a linear fit (dashed line) and a fit according to Eq. (12) (full line) are given, too.

Analyzing the initial slope of the magnetization-recovery curves is feasible for all curves as the corresponding regression analysis is numerically more stable. The results of these fits are plotted in Fig. 8. In the same figure, also a fit of the linear relationship derived in Eq. (14) is given. From the slope of the curve, a diffusion coefficient of $(3.03 \pm 0.09) \times 10^{-9}\,\mathrm{m^2\,s^{-1}}$ was determined. This diffusion coefficient is in a reasonable order of magnitude but nevertheless about 25% higher than good reference values from literature [16]. A possible explanation for the overestimate of the diffusion coefficient is a slight overestimation of the experimental slice thicknesses due to the approximation of the slice profiles (as there is a dependence on the square of the slice thickness, already a 12% overestimate would be sufficient for the observed deviation).

To further corroborate the results reported here, additional experiments were conducted with the water sample at elevated temperatures (where the diffusion effect is even more dominant due to longer longitudinal relaxation times and higher diffusion coefficients) and in the stronger gradient (with even thinner slice thicknesses at the same pulse angle). In all cases, the experimental data were in reasonable agreement to the Gaussian slice model. Further control experiments were conducted in a homogeneous magnetic field at the same resonance frequency where no decrease of the apparent longitudinal relaxation time could be observed. Similarly, additional experiments on a high molecular weight PDMS melt

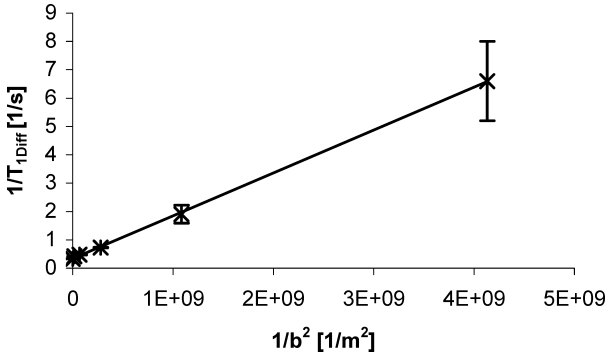

Fig. 8. Effective longitudinal relaxation rates $1/T_{1\mathrm{Diff}}$ determined from the initial slopes of the magnetization-recovery curves given in Fig. 7. The linear fit (over six data points) according to the linear relationship in Eq. (14) leads to a diffusion coefficient of $D = (3.03 \pm 0.09) \times 10^{-9}\,\mathrm{m^2\,s^{-1}}$, a longitudinal relaxation time T_1 in absence of diffusion of (2.97 ± 0.23) s and a correlation coefficient of 0.9996.

($D = 2.0 \times 10^{-12}\,\mathrm{m^2\,s^{-1}}$ according to a stimulated echo SFG diffusion measurement, $T_1 = 1\,\mathrm{s}$) placed in the gradient magnet did not show a significant influence of the slice thickness on the measured longitudinal relaxation time. This again is expected on the basis of our theory.

5. Implications for slice-selective NMR experiments

Many NMR experiments involve slice-selective excitation of magnetization. In addition to all variants of conventional magnetic resonance imaging, this is also the case for most suggested schemes in mechanically detected magnetic resonance [18,19] and for static field gradient NMR diffusometry [5].

In the following, we want to review the possible impact of the effects presented in this paper on the different experiments described here:

In static field gradient (SFG) NMR diffusometry, a stimulated echo sequence or a 5-pulse sequence (for compensation of possible transverse relaxation effects, see, e.g. [8]) are applied. The time interval τ between the first and the second 90°-pulse of the stimulated echo is much shorter than the period t_D in which the spin magnetization is stored in longitudinal orientation before initiating the stimulated echo with the third pulse. The excited slice of the sample is typically quite thin (on the order of several 100 μm) as a higher excitation bandwidth cannot be realized in the strong static magnetic field gradients. While there are in principle diffusive balancing effects in all three time intervals of the stimulated echo, the diffusion balance during the τ intervals can be neglected under typical SFG diffusometry conditions. In the much longer time interval t_D between the second and the third pulse this is not the case. Here, the magnetization available for formation of the stimulated echo will decrease with the same additional factor $B(t_D)$ which also describes the loss of magnetization due to diffusion balance effects in the saturation-recovery experiment. The overall signal attenuation is then given as:

$$S(\tau, t_D) = \frac{M_0}{2} \mathrm{e}^{-(2\tau/T_2 + t_D/T_1)} B(t_D) \mathrm{e}^{-\gamma^2 G^2 D \tau^3 \left(\frac{2}{3} + \frac{t_D}{\tau}\right)}. \qquad (15)$$

As the time interval between the second and the third pulse is typically kept constant during an SFG experiment in order to achieve a well-defined diffusion time, the influence of this balancing is the same for all τ values used in the experiment and $B(t_D)$ only leads to a reduction in the available signal amplitude but does not affect the determination of the diffusion coefficient. In the case of an experiment where t_D is varied, $B(t_D)$ is not a constant factor any more and may need to be considered in evaluating the diffusion coefficient. In a multicomponent system, $B(t_D)$ leads to different weighting of the individual components in the average diffusion coefficient determined in the SFG experiment. Fast-diffusion components will be weighted lower with increasing diffusion time t_D in this case.

The best way to minimize diffusion balance effects in an SFG experiment is to excite as thick sample slices as possible (which is of course done anyway for signal/noise considerations); nevertheless it seems indicated to take the effect into account as a possible source of difficulties in SFG experiments.

The situation in MRI experiments is different from SFG: Here, this excited sample slices are not the result of bandwidth limitations but experimentally intended in order to achieve a high spatial resolution. This is especially the case in magnetic resonance microscopy. The role of in-plane diffusion effects as a limiting factor in spatial resolution has been carefully analyzed by various authors [13,20]. Possible diffusion effects on longitudinal magnetization have not received much attention up to now. However, we find diffusion-induced changes in the apparent longitudinal relaxation behavior of water in excited slices on the order of several 100 μm. Such slice thicknesses are quite typical in state-of-the-art NMR microscopy and even thinner slices have been used in STRAFI [21,22]. Therefore, effects of diffusion on T_1 contrast in NMR microscopy may need to be considered for samples in which free long-range diffusion of water is possible. In a sample with spatially varying diffusion properties, this effect leads to a superposition of diffusive effects with T_1 contrast. The extent to which this may happen does not only depend on slice thickness, diffusion coefficient, and T_1 but also on the way the T_1 contrast is implemented in the imaging protocol: As the same slice is excited cyclically in most imaging sequences, we can expect a smaller impact of diffusion than the one calculated here as there is partially excited magnetization from earlier excitation cycles outside the slice that may diffuse back during later cycles. The shorter the repetition time in the experiment is, the more will such "old" magnetization will influence the balance factor. The resulting steady state of magnetization distribution inside and outside the excited slice and the kinetics of approaching this stage will be explored in more detail in a separate paper.

Imaging much thinner slices than in conventional MRI may be realized by mechanically detected NMR (magnetic resonance force microscopy, MRFM) in the future [18,19]. Here, diffusion effects will be even more prominent. Estimating the apparent longitudinal relaxation time of water ($T_1 = 3\,\mathrm{s}$, $D = 2.3 \times 10^{-9}\,\mathrm{m^2\,s^{-1}}$) for a 1 μm Gaussian sample slice on the basis of Eq. (14), we find a value of 0.87 ms! On the one hand, such a fast magnetization recovery in a thin excited slice may open up possibilities for new magnetization modulation schemes that could not be applied on the basis of the typical bulk relaxation times. On the other hand, a dominance of diffusion effects over the well-known bulk relaxation time values would complicate the interpreta-

tion of image contrasts obtained under such conditions. However, as already discussed in the context of conventional MRI, we must take into account the fact that magnetization modulation schemes in mechanically detected NMR involve cyclic excitations (possibly with repetition times in the sub-ms range) and so again the steady state of the magnetization must be analyzed. Furthermore, MRFM will be especially attractive for thin samples so that even the geometrical restriction of magnetization diffusion on the physical boundaries of the sample must be considered in a full analysis of this problem, too.

Comparing the performance of the diffusion measurement via the slice-thickness dependence of the apparent longitudinal relaxation time to other approaches in NMR diffusometry, there is no obvious case in which this effect offers advantages over the established approaches. However, considering the very thin slices achievable in mechanically detected NMR, the effect may offer an attractive option for diffusometry on the μm (or even sub-μm) scale in thin sample layers or nanofluidic systems. Furthermore, the effect should be considered as a possible source of systematical experimental errors when measuring longitudinal relaxation times in inhomogeneous magnetic fields.

Acknowledgments

The authors gratefully acknowledge the access to all laboratory equipment of the Fujara group. B.W. was involved into the work under the auspices of the Polish-German-Dialogue programme 2003. N.N. was funded by a special initiative of the BMBF for the establishment of independent junior research groups (“Juniorprofessuren”). N.N. furthermore acknowledges stimulating discussions with D. Kruk and F. Fujara.

References

[1] E. Hahn, Spin echoes, Physical Review 80 (1950) 580–594.
[2] E.O. Stejskal, J.E. Tanner, Spin diffusion measurements: spin echoes in the presence of a time-dependent field-gradient, Journal of Chemical Physics 42 (1965) 288–292.
[3] J.E. Tanner, Use of stimulated echo in NMR diffusion studies, Journal of Chemical Physics 52 (1970) 2523–2526.
[4] J. Kärger J, W. Heink, The propagator representation of molecular transport in microporous crystallites, Journal of Magnetic Resonance 51 (1983) 1–7.
[5] G. Fleischer, F. Fujara, Segmental diffusion in polymer melts and solutions of poly(ethylene oxide) measured with field gradient NMR in high-field gradients, Macromolecules 25 (1992) 4210–4212.
[6] P. Galvosas, F. Stallmach, G. Seiffert, J. Kärger, U. Kaess, G. Majer, Generation and application of ultra-high-intensity magnetic field gradient pulses for NMR spectroscopy, Journal of Magnetic Resonance 151 (2001) 260–268.
[7] S. Braun, H.O. Kalinowski, S. Berger, 150 and More Basic NMR Experiments, VCH:Weinheim, 1998.
[8] R. Kimmich, NMR-Tomography, Diffusometry, Relaxometry, Springer, Heidelberg, 1997.
[9] B. Blümich, NMR Imaging of Materials, Clarendon Press, Oxford, 2000.
[10] R. Kimmich, B. Simon, H. Koestler, Magnetization grid rotating-frame imaging technique for diffusion and flow measurements, Journal of Magnetic Resonance A 112 (1994) 7–12.
[11] E.E. Sigmund, W.P. Halperin, Hole-burning diffusion measurements in high magnetic field gradients, Journal of Magnetic Resonance 163 (2003) 99–104.
[12] Presentation by D. Canet at the XI AMPERE NMR summer school, Zakopane, Poland, 2003.
[13] P.T. Callaghan, Principles of Magnetic Resonance Microscopy, Clarendon Press, Oxford, 1991.
[14] J. Crank, The Mathematics of Diffusion, Clarendon Press, Oxford, 1956.
[15] I. Chang, F. Fujara, B. Geil, G. Hinze, H. Sillescu, A. Tölle, New perspectives of NMR in ultrahigh static magnetic field gradients, Journal of Non-Crystalline Solids 172 (1994) 674–681.
[16] M. Holz, S.R. Heil, A. Sacco, Temperature-dependent self-diffusion coefficients of water and six selected molecular liquids for calibration in accurate ^{1}H NMR PFG measurements, Physical Chemistry Chemical Physics 2 (2000) 4740–4742.
[17] Available from www.python.org.
[18] J.A. Sidles, Noninductive detection of single-proton magnetic resonance, Applied Physics Letters 58 (1991) 2854–2856.
[19] N. Nestle, A. Schaff, W.S. Veeman, Mechanically detected NMR, an evaluation of the applicability for chemical investigations, Progress in Nuclear Magnetic Resonance Spectroscopy 38 (2001) 1–35.
[20] A. Haase, M. Brandl, E. Kuchenbrod, A. Link, Magnetization-prepared NMR microscopy, Journal of Magnetic Resonance Series A 105 (1993) 230–233.
[21] A.A. Samoilenko, D.Y. Artemov, L.A. Sibeldina, Formation of sensitive layer in experiments on NMR subsurface imaging of solids, JETP Letters 47 (1988) 417–419.
[22] P. McDonald, Stray field magnetic resonance imaging, Progress in NMR Spectroscopy 30 (1997) 69–99.